Coherent Manipulation of Coupled Electron Spins in Semiconductor Quantum Dots

J. R. Petta,[1] A. C. Johnson,[1] J. M. Taylor,[1] E. A. Laird,[1] A. Yacoby,[2] M. D. Lukin,[1] C. M. Marcus,[1] M. P. Hanson,[3] A. C. Gossard[3]

We demonstrated coherent control of a quantum two-level system based on two-electron spin states in a double quantum dot, allowing state preparation, coherent manipulation, and projective readout. These techniques are based on rapid electrical control of the exchange interaction. Separating and later recombining a singlet spin state provided a measurement of the spin dephasing time, T_2^*, of ~10 nanoseconds, limited by hyperfine interactions with the gallium arsenide host nuclei. Rabi oscillations of two-electron spin states were demonstrated, and spin-echo pulse sequences were used to suppress hyperfine-induced dephasing. Using these quantum control techniques, a coherence time for two-electron spin states exceeding 1 microsecond was observed.

Quantum coherence and entanglement have emerged as physical bases for information-processing schemes that use two-state quantum systems (quantum bits or qubits) to provide efficient computation and secure communication (*1*, *2*). Although quantum control of entanglement has been realized in isolated atomic systems, its extension to solid-state systems—motivated by the prospect of scalable device fabrication—remains a demanding experimental goal (*3*, *4*), particularly because of the stronger coupling of solid-state qubits to their environment. Understanding this coupling and learning how to control quantum systems in the solid state is a major challenge of modern condensed-matter physics (*5*, *6*).

An attractive candidate for a solid-state qubit is based on semiconductor quantum dots, which allow controlled coupling of one or more electrons, using rapidly switchable voltages applied to electrostatic gates (*7*–*9*). Recent experiments suggest that spin in quantum dots may be a particularly promising holder of quantum information, because the spin relaxation time (T_1) can approach tens of milliseconds (*10*–*13*). Although gallium arsenide (GaAs) is a demonstrated exceptional material for fabricating quantum dots, it has the potential drawback that confined electrons interact with on the order of 10^6 spin-3/2 nuclei through the hyperfine interaction. Here we present a quantum two-level system (logical qubit) based on two-electron spin states (*14*) and demonstrate coherent control of this system through the use of fast electrical control of the exchange interaction. We first show by direct time-domain measurements that the time-ensemble-averaged dephasing time (T_2^*) of this qubit is ~10 ns, limited by hyperfine interactions. We then demonstrate Rabi oscillations in the two-spin space (including a 180-ps $\sqrt{\text{SWAP}}$ operation between two electron spins) and implement spin-echo sequences, showing an extended spin coherence time, T_2, beyond 1 μs.

Isolating and measuring two electrons. Gate-defined double quantum dot devices are fabricated using a GaAs/AlGaAs heterostructure grown by molecular beam epitaxy with a two-dimensional electron gas 100 nm below the surface, with density ~2×10^{11} cm^{-2}. When biased with negative voltages, the patterned gates create a double-well potential (Fig. 1A). Tunnel barriers [controlled by voltages V_L and V_R (L, left; R, right)] connect each dot to adjacent reservoirs, allowing electrons to be transferred into the dots. Interdot tunneling (at a rate set by voltage V_T) allows electrons to be moved between dots when the detuning parameter $\varepsilon \propto V_R - V_L$ is adjusted. Measurements are performed in a dilution refrigerator with electron temperature T_e ~ 135 mK, determined from Coulomb blockade peak widths. Gates L and R are connected via low-temperature bias tees to high-bandwidth coaxial lines, allowing rapid (~1 ns) pulsing of these gates (*15*). High-frequency manipulation of a single electron, demonstrating the gigahertz bandwidth of this setup, was reported in (*16*).

Quantum point contact (QPC) sensors fabricated next to each dot serve as local electrometers (*17*, *18*), showing a few-percent reduction of conductance when a single charge is added to the adjacent dot. Figure 1B shows the conductance, g_s, of the right QPC sensor as a function of V_L and V_R near the two-electron regime. Each charge state gives a distinct value of g_s, decreasing each time an electron is added to the system or when an electron is transferred from the left dot to the right dot. Labels (m,n) in each region indicate the absolute number of electrons confined on the (left, right) dot in the ground state. We focus on transitions involving (0,2) and (1,1) two-electron states, where previous experiments have demonstrated spin-selective tunneling (*12*, *13*, *19*, *20*).

Voltage-controlled exchange. The relative energy detuning ε of the (0,2) and (1,1) charge states can be rapidly controlled by

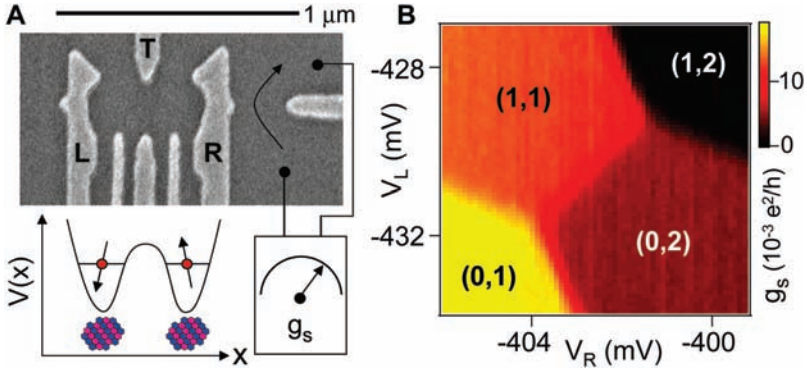

Fig. 1. (**A**) Scanning electron micrograph of a sample identical to the one measured, consisting of electrostatic gates on the surface of a two-dimensional electron gas. Voltages on gates L and R control the number of electrons in the left and right dots. Gate T is used to adjust the interdot tunnel coupling. The quantum point contact conductance g_s is sensitive primarily to the number of electrons in the right dot. (**B**) g_s measured as a function of V_L and V_R reflects the double-dot charge stability diagram (a background slope has been subtracted). Charge states are labeled (m,n), where m is the number of electrons in the left dot and n is the number of electrons in the right dot. Each charge state gives a distinct reading of g_s.

[1]Department of Physics, Harvard University, Cambridge, MA 02138, USA. [2]Department of Condensed Matter Physics, Weizmann Institute of Science, Rehovot 76100, Israel. [3]Materials Department, University of California at Santa Barbara, Santa Barbara, CA 93106, USA.

applying calibrated voltage pulses to gates L and R (Fig. 2B). For $\varepsilon > 0$, the ground-state charge configuration is (0,2). Tight confinement in (0,2) favors a spin-singlet configuration, denoted (0,2)S. The corresponding (0,2) triplet states are energetically inaccessible, lying ~400 μeV above (0,2)S and are neglected in the following discussion. For $\varepsilon < 0$, the ground state configuration is (1,1). In this case, four spin states are accessible: the singlet (S = 0), denoted S [suppressing the (1,1) label]; and three triplets (S = 1), denoted T_-, T_0, and T_+, corresponding to $m_s = -1, 0, +1$.

In the absence of interdot tunneling, the two spins in the (1,1) configuration are independent; that is, S, T_0, T_+, and T_- are degenerate. At finite magnetic fields, S and T_0 are degenerate. When interdot tunneling is present, the (0,2) and (1,1) charge states hybridize, which results in an exchange splitting $J(\varepsilon)$ between the S and T_0 spin states of (1,1) that depends on detuning (Fig. 2B). Near zero detuning, exchange J ($\varepsilon \rightarrow 0$) becomes large (equal to half the splitting of symmetric and antisymmetric charge states at $\varepsilon = 0$); for large negative detuning, $\varepsilon \ll -J(0)$, exchange vanishes, $J(\varepsilon) \rightarrow 0$, and the spins again become independent. Except where noted, a perpendicular magnetic field $B = 100$ mT is used to split off the $T_\pm$ states from T_0 by the Zeeman energy $E_z = \pm g^*\mu_B B \sim 2.5$ μeV ($g^* = -0.44$ is the electron g factor in GaAs; μ_B is the Bohr magneton). The split-off T_+ state crosses the hybridized singlet S when $J(\varepsilon) = g^*\mu_B B$ (vertical green line in Fig. 2B), allowing $J(\varepsilon)$ to be readily measured, as discussed below.

In all measurements, a cyclical pulse sequence is used (see Fig. 2A for a schematic representation). A pulse transfers the (0,2)S state into the spatially separated (1,1) singlet state, S. The singlet state is manipulated with various control techniques (discussed below). After manipulation, the resulting (1,1) spin state is projected back onto (0,2)S for a measurement of the singlet probability P_S. P_S is measured with the QPC: the T states of (1,1) remain in a spin-blocked configuration, whereas the S state tunnels directly to (0,2)S. This spin-to-charge conversion readout is based on the same mechanism that results in rectification in dc transport found in similar devices (*19*, *20*). The majority of the duty cycle is spent in the measurement configuration ($\varepsilon > 0$), so that the slow (time-averaged) measurement of the QPC conductance reflects the charge configuration during the measurement phase (*12*, *13*).

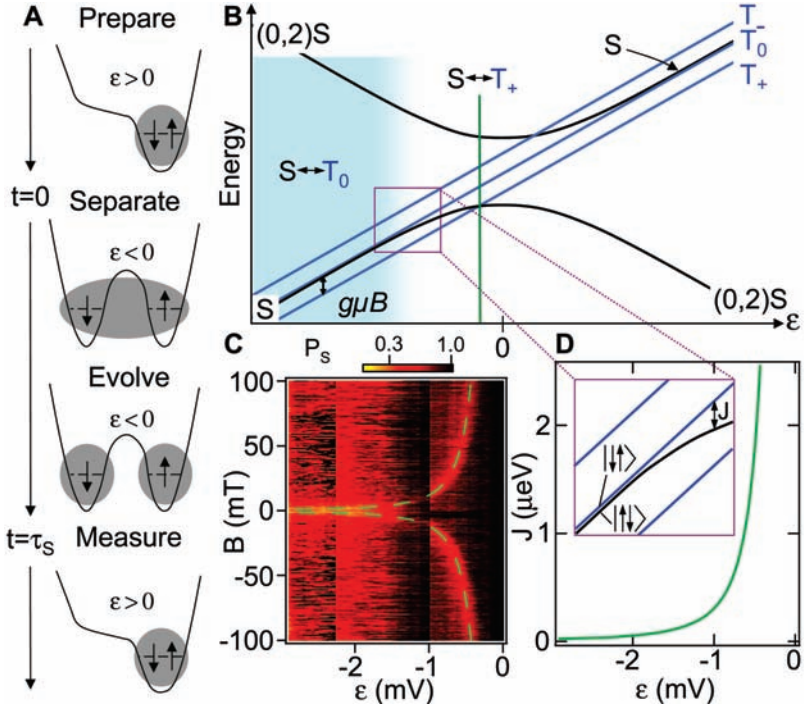

Fig. 2. (**A**) The control cycle for experiments generally consists of preparation, singlet separation, evolution of various kinds, and projection onto the (0,2) singlet state (measurement). Projective measurement is based on the spin-blockaded transition of T states onto (0,2)S, whereas S states proceed freely, allowing S to be distinguished from T by the charge sensor during the measurement step. (**B**) Energy diagram near the (1,1)-to-(0,2) charge transition. A magnetic field splits T states by the Zeeman energy. At the S-T_0 degeneracy (light blue region) and the S-T_+ degeneracy (green line), hyperfine fields drive evolution between S and the respective T states. (**C**) Singlet probability P_S after $\tau_s = 200$ ns, as a function of detuning ε and magnetic field B maps out degeneracies of S-T_0 ($\varepsilon < \sim -1.2$ mV) and S-T_+ (dashed green curve). (**D**) Dependence of exchange on detuning, extracted from the fit of $J(\varepsilon) = g^*\mu_B B$ along the S-T_+ resonance, assuming $g^* = -0.44$ [dashed curve in (C)]. (Inset) For $J(\varepsilon) \gg g^*\mu_B B_{nuc}$, eigenstates S and T_0 are split by $J(\varepsilon)$. At large negative detuning, $J(\varepsilon) \ll g^*\mu_B B_{nuc}$, and S and T_0 are mixed by hyperfine fields but eigenstates $|\uparrow\downarrow\rangle$ and $|\downarrow\uparrow\rangle$ are not.

Even though we can coherently control and measure two-electron spin states electrically, the local solid-state environment remains critically important. For our device, each electron is coupled to roughly 10^6 GaAs nuclei through the hyperfine interaction. The hyperfine interaction results in an effective random magnetic field with magnitude $B_{nuc} \sim 1$ to 5 mT (*13*, *21*, *22*). These random hyperfine fields evolve slowly (>10 μs) relative to typical pulse sequence periods and result in spin dephasing, thereby coupling two-electron spin states (*23*–*28*). At large negative detuning, where $J(\varepsilon) < g^*\mu_B B_{nuc}$, these effective fields mix S and T states.

The logical qubit. With the $T_\pm$ states split off by an applied field $B \gg B_{nuc}$, the states S and T_0 form an effective two-level system (or qubit) with Hamiltonian

$$H = \begin{pmatrix} J(\varepsilon) & \Delta B^z_{nuc} \\ \Delta B^z_{nuc} & 0 \end{pmatrix}$$

where ΔB^z_{nuc} is the difference in random hyperfine fields along the applied field direction. To facilitate the following discussion, we define a Bloch sphere for the S-T_0 two-level system that has S and T_0 at the north and south poles (z axis) and the eigenstates of the instantaneous nuclear fields within this subspace, $|\uparrow\downarrow\rangle$ and $|\downarrow\uparrow\rangle$, as the poles along the x axis (Fig. 3A).

Dephasing of the separated singlet. The pulse sequence described in Fig. 3A is used to measure the dephasing of the separated singlet state as a function of the time τ_S that the system is held at large detuning [with $J(\varepsilon) < g^*\mu_B B_{nuc}$]. This time is a T_2^* time (the asterisk indicates an average over many experimental runs), because relative phase evolution of the separated spins can convert the initial singlet into a triplet, which will not be able to return to (0,2)S. The (0,2)S initial state is prepared each cycle by allowing tunneling to the reservoir with (0,2)S below the Fermi level of the leads and the (0,2) triplets above. This energetic configuration is held for 200 ns, and through a process in which an electron is exchanged with the leads, (0,2)S is prepared. The state is then separated into (1,1) using rapid adiabatic passage, where ε is swept from a positive value to a large negative value quickly (~1 ns) relative to the nuclear mixing time $\sim \hbar/(g^*\mu_B B_{nuc})$ but slowly as compared to the tunnel splitting of the hybridized charge states $\sim \hbar/J(0)$. This yields a separated singlet, S. After a separation time τ_S, the state is projected back onto (0,2)S, again using rapid adiabatic passage, and the system is held at the measurement point for a time $\tau_M \sim 5$ to 10 μs < T_1.

The average singlet probability measured after a separation time of 200 ns, $P_S(\varepsilon, B, \tau_S = 200$ ns), is shown in Fig. 2C as a function of

detuning at the separation point and applied field (*29*). Evident in the data are a funnel-shaped feature where S and T_+ cross (vertical green line in Fig. 2B) and are rapidly mixed by hyperfine fields. The degeneracy occurs at $J(\varepsilon) = g^*\mu_B B$, allowing $J(\varepsilon)$ to be measured (Fig. 2D) by mapping the location of this feature in $P_S(\varepsilon,B)$. At larger detuning, where $J(\varepsilon) < g^*\mu_B B_{nuc}$, the S and T_0 states approach degeneracy and are susceptible to hyperfine mixing, which reduces P_S (light blue area of Fig. 2B). When $B < B_{nuc}$, all three degenerate triplet states can mix with S at large detuning, which further reduces P_S as compared to the finite-field case.

For applications involving the manipulation of entangled pairs of electrons, a relevant question is how long the electrons can be spatially separated before losing phase coherence. We measure this time by varying the singlet separation time τ_S. The time evolution of the average singlet return probability, $P_S(\tau_S)$, measured using the pulse sequence in Fig. 3A with $\varepsilon = -6$ mV, is shown in Fig. 3B. As τ_S increases, P_S decreases from ~1 on a 10-ns time scale, saturating after 20 ns to $P_S \sim 0.5$ (0.7) for $B = 0$ (100) mT.

A semiclassical model of dephasing of the separated singlet was investigated in (*23*). It assumes independent quasistatic nuclear fields acting on the two spins (*26*, *30*) and ideal measurement contrast, and yields Gaussian-like decay on a time scale T_2^* from $P_S(\tau_S = 0) = 1$ to long-time saturating values $P_S(\tau_S \gg T_2^*) = 1/3$ for $B \ll B_{nuc}$ and $P_S(\tau_S \gg T_2^*) = 1/2$ at $B \gg B_{nuc}$. The field dependence is caused by the lifting of the triplet degeneracy with the external field, although the naïve expectation based on incoherent mixing would be $P_S(\tau_S \gg T_2^*) = 1/4$, not 1/3, at $B = 0$. Fits to the measured $P_S(\tau_S)$ yield $T_2^* = 10 \pm 1$ ns, corresponding to $B_{nuc} = 2.3$ mT, consistent with previous measurements (*13*, *22*, *31*). An observed ~40% reduction of contrast is treated as a fit parameter. The predicted weak overshoot of P_S for $B = 0$, a remnant of Rabi oscillations (*23*), is not seen in these data.

Spin SWAP and Rabi oscillations in the $|\uparrow\downarrow\rangle$, $|\downarrow\uparrow\rangle$ basis. By initializing from (0,2)S using slow ramping of detuning, the (1,1) system can be initialized into the ground state of the nuclear field [defined as $|\uparrow\downarrow\rangle$ (Fig. 2D, inset)] instead of the singlet state S. This initialization scheme is illustrated in Fig. 4A: after preparing (0,2)S (as described above), detuning is swept to $\varepsilon < 0$ slowly relative to tunnel splitting but quickly relative to the nuclear mixing time through the S-T_+ degeneracy. The system is then ramped slowly as compared to the nuclear mixing time ($\tau_A \sim 1\ \mu s \gg T_2^*$) to large negative detuning. This slow lowering of $J(\varepsilon)$ leads to adiabatic following of the initial state S into the state $|\uparrow\downarrow\rangle$, the ground state of the Hamiltonian with $J \to 0$ (*30*, *32*). Readout follows the same steps in reverse: ramping slowly out of the large detuning region unloads $|\uparrow\downarrow\rangle$ to S and $|\downarrow\uparrow\rangle$ to T_0. Then, moving quickly though S-T_+ degeneracy and finally projecting onto (0,2)S measures the fraction that was in the state $|\uparrow\downarrow\rangle$ before readout.

Once initialized in $|\uparrow\downarrow\rangle$, the application of a finite exchange $J(\varepsilon)$ for a time τ_E rotates the spin state about the z axis of the Bloch sphere, in the plane containing $|\uparrow\downarrow\rangle$ and $|\downarrow\uparrow\rangle$, through an angle $\phi = J(\varepsilon)\tau_E/\hbar$. The case $J(\varepsilon)\tau_E/\hbar = \pi$ constitutes a SWAP operation, rotating the state $|\uparrow\downarrow\rangle$ into the state $|\downarrow\uparrow\rangle$.

Figure 4B shows $P_S(\varepsilon,\tau_E)$ oscillating as a function of both τ_E and ε, with minima of the singlet probability corresponding to $J(\varepsilon)\tau_E/\hbar = \pi, 3\pi, 5\pi,\ldots$. The inset shows theoretical predictions $P_S = \{1 + \cos[J(\varepsilon)\tau_E/\hbar]\}/2$, using values for $J(\varepsilon)$ obtained independently from the S-T_+ resonance measurement as in Fig. 2C. In Fig. 4C, we plot exchange oscillations at the four values of detuning marked by the dashed lines in Fig. 4B. Data are fit using an exponentially damped cosine with offset, amplitude, decay time, and phase as fit parameters. To achieve faster π-pulse times, $J(\varepsilon)$ can be increased by setting V_T to increase interdot tunnel coupling and by moving to less negative (or even positive) detunings during the exchange pulse (Fig. 4D). The fastest π-pulse time obtained using these methods is ~350 ps (*33*).

We note that the observed decay time of Rabi oscillations is proportional to the Rabi period, suggesting that dephasing scales with the value of $J(\varepsilon)$ during the exchange pulse and may reflect gate noise during the τ_E interval. The contrast (~45%) seen in Fig. 4, B and C, is consistent with the contrast obtained in the singlet separation measurement of T_2^*.

Singlet-triplet spin-echo. Voltage-controlled exchange provides a means of refocusing the separated singlet to undo dephasing due to the local hyperfine fields. The pulse sequence is shown in Fig. 5A and is similar to refocusing sequences used in nuclear magnetic resonance (*34*, *35*). The separated singlet S will dephase at large negative detuning [$J(\varepsilon) \sim 0$] due to local hyperfine fields after a separation time τ_S. In the Bloch sphere representation, hyperfine dephasing results in a rotation by a random nuclear-field–dependent angle about the x axis. Thus, in each run the Bloch vector rotates by a random amount about the x axis. The dephased (1,1) state can be refocused to S by applying a pulse of finite exchange $J(\varepsilon)$ for a time τ_E, where $J(\varepsilon)\tau_E/\hbar = \pi, 3\pi, 5\pi,\ldots$, which rotates the Bloch vector around the z axis by an angle $\pi, 3\pi, 5\pi,\ldots$, and waiting for a time $\tau_S' = \tau_S$.

The singlet probability $P_S(\varepsilon,\tau_E)$ measured using the spin-echo sequence (Fig. 5A) is shown as a function of detuning and τ_E in Fig. 5B. Singlet recoveries (black regions) are observed for π, 3π, and 5π exchange pulses. A plot of the theoretical prediction $P_S = \{3 - \cos[J(\varepsilon)\tau_E/\hbar]\}/4$ (Fig. 5B, inset) using values

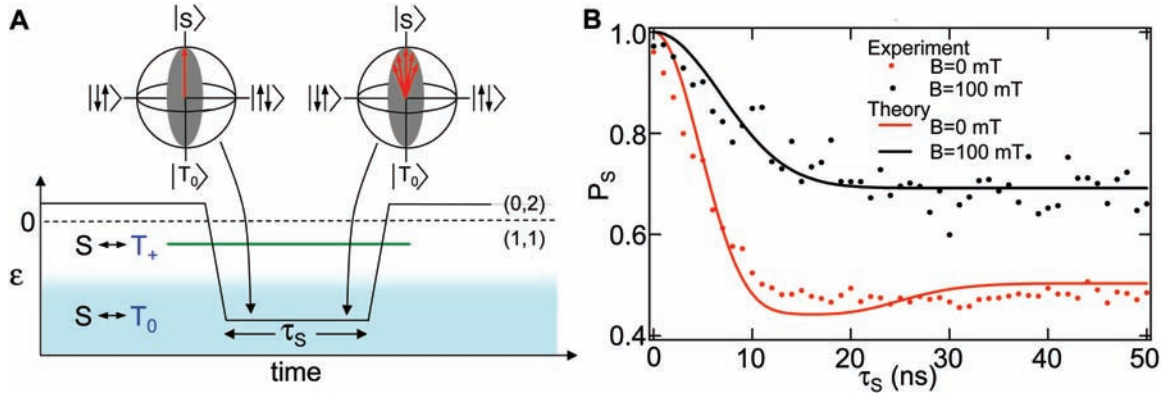

Fig. 3. (**A**) Pulse sequence used to measure T_2^*. The system is initialized into (0,2)S and transferred by rapid adiabatic passage to the spatially separated S state. With $T_\pm$ separated by a Zeeman field, S and T_0 mix at large detuning (light blue region), where hyperfine fields drive rotations about the x axis in the Bloch sphere. After a separation time τ_S, the state is projected onto (0,2)S. (**B**) Singlet probability P_S measured using the calibrated QPC charge sensor, as a function of τ_S at 100 mT (black curve) and 0 mT (red curve). For $\tau_S \ll T_2^*$, the singlet state does not have ample time to dephase, and $P_S \sim 1$. For $\tau_S \gg T_2^*$, $P_S \sim 0.7$ at 100 mT and $P_S \sim 0.5$ at 0 mT. A semiclassical model of dephasing due to hyperfine coupling (*23*) predicts $P_S \sim 1/2$ at high field and $P_S \sim 1/3$ at zero field. Fits to the model (solid curves), including a parameter adjusting measurement contrast, give $T_2^* = 10$ ns and $B_{nuc} = 2.3$ mT.

for $J(\varepsilon)$ measured independently from the S-T_+ resonance condition compares well with experiment. We note greater noise in these data than in Fig. 4. We speculate that this noise, which is ~100 times noisier than the QPC sensor readout instrument noise, is likely due to slow fluctuations in the nuclear system. Noise from a possibly similar origin was recently observed in dc transport through a double quantum dot system (*36*). Figure 5C shows P_S (red) as a function of the difference in dephasing and rephasing times, $\tau_S - \tau_S'$, for increasing values of the total time spent at large detuning, $\tau_S + \tau_S'$, averaged over 10 data sets. Differences in τ_S and τ_S' result in imperfect refocusing and decrease the recovery amplitude on a characteristic time scale $\tau_S - \tau_S' = T_2^*$.

For each value of $\tau_S + \tau_S'$, the data are fit to a Gaussian form giving $T_2^* = 9 \pm 2$ ns, consistent with measurements of the singlet decay discussed above. The best-fit heights for each $\tau_S + \tau_S'$ time are plotted as the black data points in Fig. 5C. A fit to an exponential decay with an adjustable offset to correct for the finite measurement contrast gives a characteristic coherence time of 1.2 μs, which sets a lower bound on T_2. Comparing measured values of T_2^* and this bound on T_2, we note that a simple spin-echo sequence extends the coherence time of a spatially separated singlet by more than a factor of 100. We find that two spin-echo pulse sequences applied in series (Carr-Purcell) extends the bound on T_2 by at least another factor of 2. The coherence time of our qubit using the simple spin-echo sequence exceeds the $\sqrt{\text{SWAP}}$ operation time by a factor of ~7000. Because the echo sequence relies on gate-voltage control of $J(\varepsilon)$, it is susceptible to charge dephasing during the exchange pulse. The interplay between charge dephasing during the exchange pulse and dephasing due to nuclear processes warrants further investigation (*30*, *37*).

Summary and outlook. We have demonstrated coherent quantum control of a logical qubit based on two-electron spin states. Spin states are prepared, manipulated, and measured using fast control of the exchange interaction. Rapid electrical control of the exchange interaction is used to measure T_2^*, to demonstrate Rabi oscillations and a 180-ps $\sqrt{\text{SWAP}}$ operation, and to greatly reduce dephasing of a spatially separated spin-singlet state with spin-echo techniques. Moreover, the echo sequence implements a dynamical decoherence-free subspace (*38*, *6*), which allows arbitrary two-electron spin states in S-T_0 subspace to be protected from noise. Furthermore, our results show that even in the presence of dephasing, such an encoded logical qubit can be manipulated efficiently with effectively long coherence times. This two-electron spin qubit may provide a starting point for implementation of quantum computation schemes with considerable practical advantages: All operations for preparing, protecting, and measuring entangled electron spins can be implemented by local electrostatic gate control. We anticipate that the techniques developed in this work will lead to intriguing prospects for experimental realizations of ideas from quantum information science in semiconductor nanostructures.

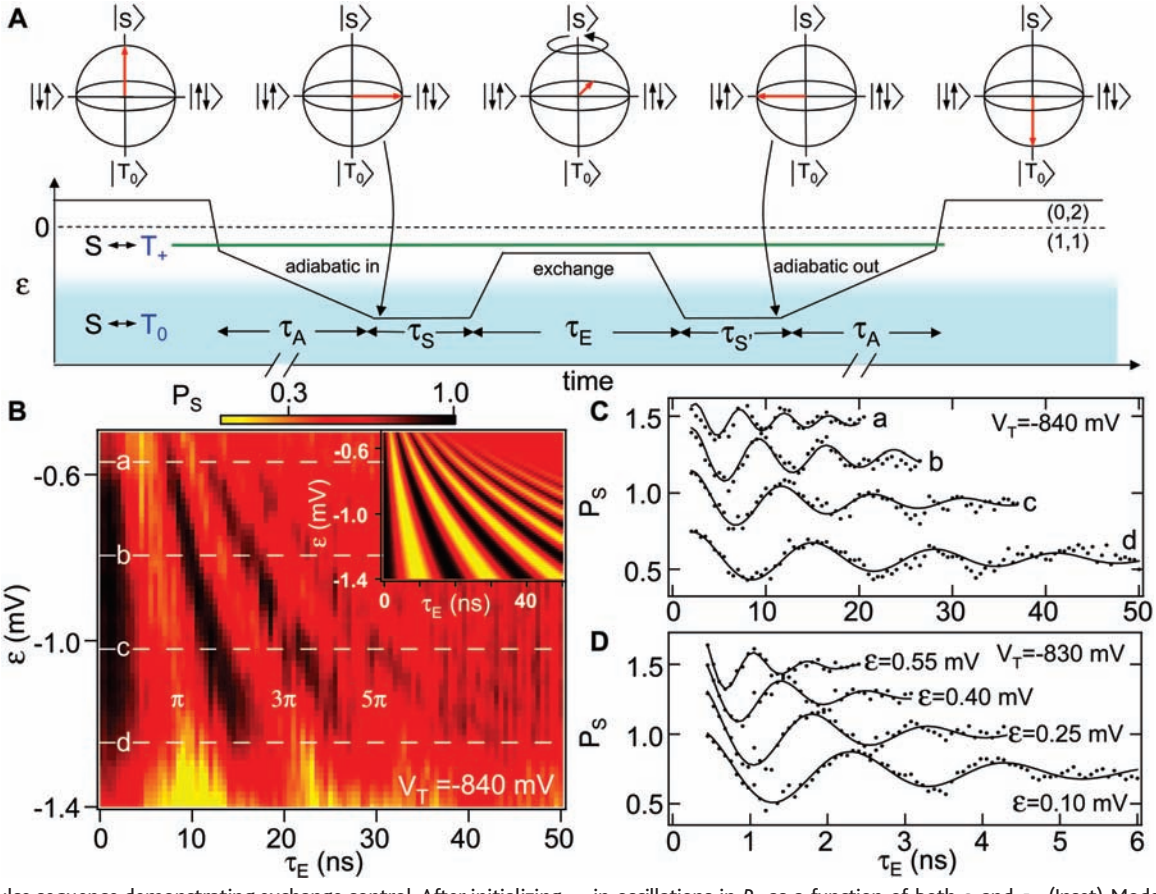

Fig. 4. (**A**) Pulse sequence demonstrating exchange control. After initializing into (0,2)S, detuning ε is swept adiabatically with respect to tunnel coupling through the S-T_+ resonance (quickly relative to S-T_+ mixing), followed by a slow ramp ($\tau_A \sim 1$ μs) to large detuning, loading the system in the ground state of the nuclear fields $|\uparrow\downarrow\rangle$. An exchange pulse of duration τ_E rotates the system about the *z* axis in the Bloch sphere from $|\uparrow\downarrow\rangle$ to $|\downarrow\uparrow\rangle$. Reversing the slow adiabatic passage allows the projection onto (0,2)S to distinguish states $|\uparrow\downarrow\rangle$ and $|\downarrow\uparrow\rangle$ after time τ_E. Typically, $\tau_S = \tau_S' = 50$ ns. (**B**) P_S as a function of detuning and τ_E. The *z*-axis rotation angle $\phi = J(\varepsilon)\tau_E/\hbar$ results in oscillations in P_S as a function of both ε and τ_E. (Inset) Model of P_S using $J(\varepsilon)$ extracted from S-T_+ resonance condition, assuming $g^* = -0.44$ and ideal measurement contrast (from 0 to 1). (**C**) Rabi oscillations measured in P_S at four values of detuning indicated by the dashed lines in (B). Fits to an exponentially damped cosine function, with amplitude, phase, and decay time as free parameters (solid curves), are shown. Curves are offset by 0.3 for clarity. (**D**) Faster Rabi oscillations are obtained by increasing tunnel coupling and by increasing detuning to positive values, resulting in a π-pulse time of ~350 ps.

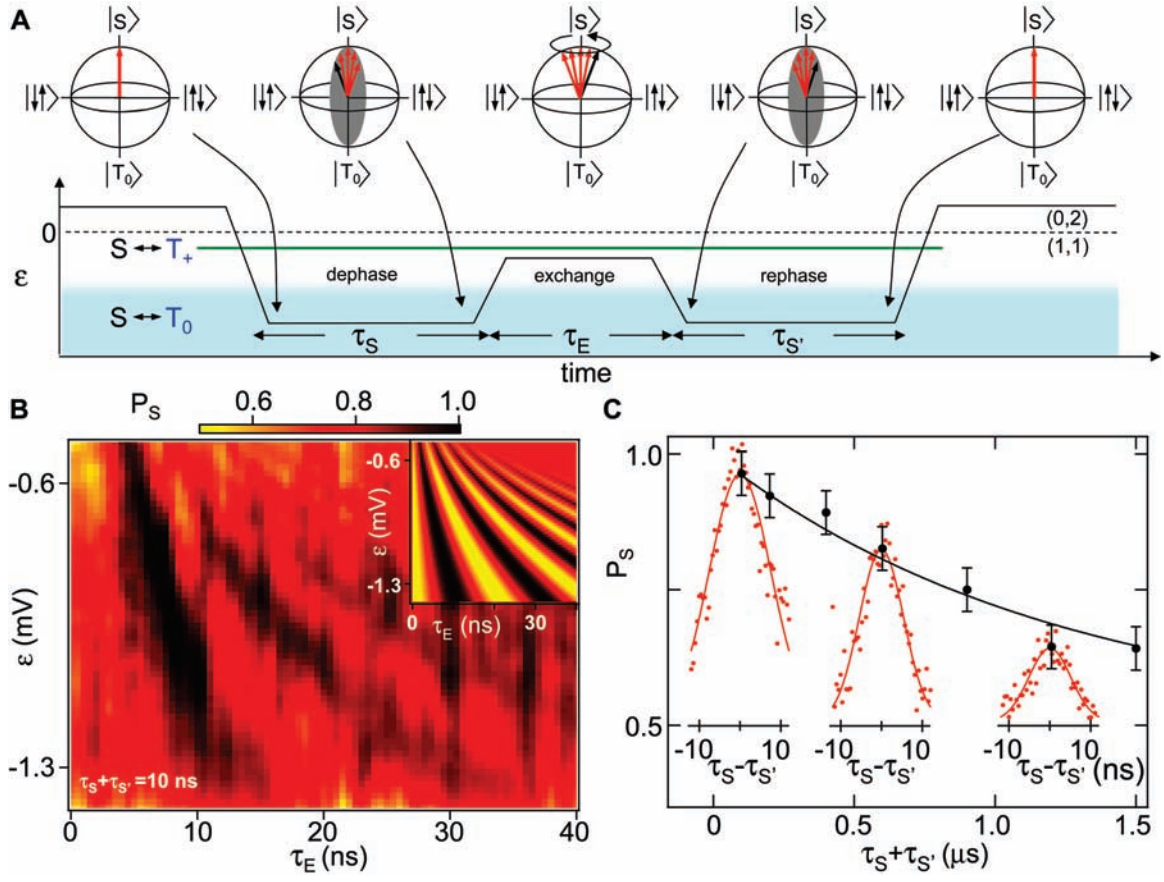

Fig. 5. (**A**) Spin-echo pulse sequence. The system is initialized in (0,2)S and transferred to S by rapid adiabatic passage. After a time τ_S at large negative detuning, S has dephased into a mixture of S and T_0 due to hyperfine interactions. A *z*-axis π pulse is performed by making detuning less negative, moving to a region with sizable $J(\varepsilon)$ for a time τ_E. Pulsing back to negative detunings for a time $\tau_S' = \tau_S$ refocuses the spin singlet. (**B**) P_S as a function of detuning and τ_E. The *z*-axis rotation angle $\phi = J(\varepsilon)\tau_E/\hbar$ results in oscillations in P_S as a function of both ε and τ_E. (Inset) Model of P_S using $J(\varepsilon)$ extracted from the S-T_+ resonance condition, assuming $g^* = -0.44$ and ideal measurement contrast (from 0.5 to 1). (**C**) Echo recovery amplitude P_S plotted as a function of $\tau_S - \tau_S'$ for increasing $\tau_S + \tau_S'$ (red points), along with fits to a Gaussian with adjustable height and width. The best-fit width gives $T_2^* = 9$ ns, which is consistent with the value $T_2^* = 10$ ns obtained from singlet decay measurements (Fig. 3B). Best-fit heights (black points) along with the exponential fit to the peak height decay (black curve) give a lower bound on the coherence time T_2 of 1.2 μs.

References and Notes

1. P. W. Shor, in *Proceedings of the 35th Annual Symposium on Foundations of Computer Science*, S. Goldwasser, Ed. (IEEE Computer Society Press, Los Alamitos, CA, 1994).
2. L. K. Grover, *Phys. Rev. Lett.* **79**, 325 (1997).
3. J. Chiaverini *et al.*, *Science* **308**, 997 (2005).
4. D. Vion *et al.*, *Science* **296**, 886 (2002).
5. A. O. Caldeira, A. J. Leggett, *Phys. Rev. Lett.* **46**, 211 (1981).
6. J. M. Taylor *et al.*, *Phys. Rev. Lett.* **94**, 236803 (2005).
7. D. Loss, D. P. DiVincenzo, *Phys. Rev. A.* **57**, 120 (1998).
8. M. Ciorga *et al.*, *Phys. Rev. B* **61**, R16315 (2000).
9. H.-A. Engel, D. Loss, *Science* **309**, 588 (2005).
10. T. Fujisawa, D. G. Austing, Y. Tokura, *Nature* **419**, 278 (2002).
11. J. M. Elzerman *et al.*, *Nature* **430**, 431 (2004).
12. J. R. Petta *et al.*, available at www.arXiv.org/abs/cond-mat/0412048 (2004).
13. A. C. Johnson *et al.*, *Nature* **435**, 925 (2005).
14. J. Levy, *Phys. Rev. Lett.* **89**, 147902 (2002).
15. Except where noted, a Tektronix AWG520 pulse generator with a 1-ns minimum pulse width was used for fast gate control. The sample response to fast pulses was checked by measuring g_s with pulses applied individually to gates L and R. A doubling of the charge stability diagram was observed for pulse widths down to 1 ns (*12*).
16. J. R. Petta, A. C. Johnson, C. M. Marcus, *Phys. Rev. Lett.* **93**, 186802 (2004).
17. M. Field *et al.*, *Phys. Rev. Lett.* **70**, 1311 (1993).
18. J. M. Elzerman *et al.*, *Phys. Rev. B* **67**, 161308 (2003).
19. K. Ono, D. G. Austing, Y. Tokura, *Science* **297**, 1313 (2002).
20. A. C. Johnson, J. R. Petta, C. M. Marcus, M. P. Hanson, A. C. Gossard, available at www.arXiv.org/abs/cond-mat/0410679 (2004).
21. D. Paget, G. Lampel, B. Sapoval, *Phys. Rev. B* **15**, 5780 (1977).
22. A. S. Bracker *et al.*, *Phys. Rev. Lett.* **94**, 047402 (2005).
23. K. Schulten, P. G. Wolynes, *J. Chem. Phys.* **68**, 3292 (1978).
24. G. Burkhard, D. Loss, D. P. DiVincenzo, *Phys. Rev. B* **59**, 2070 (1999).
25. A. V. Khaetskii, D. Loss, L. Glazman, *Phys. Rev. Lett.* **88**, 186802 (2002).
26. I. A. Merkulov, Al. L. Efros, M. Rosen, *Phys. Rev. B* **65**, 205309 (2002).
27. R. de Sousa, S. Das Sarma, *Phys. Rev. B* **68**, 115322 (2003).
28. W. A. Coish, D. Loss, *Phys. Rev. B* **70**, 195340 (2004).
29. The separation detuning can be changed by keeping pulse displacements fixed and sweeping the measurement point detuning using dc gates, or by keeping the measurement point fixed and changing pulse parameters.
30. J. M. Taylor *et al.*, in preparation.
31. The semiclassical model developed in (*23*, *30*) yields $P_S(\tau_S) = 1 - \frac{C_1}{2}\left(1 - e^{-(\tau_S/T_2^*)^2}\right)$ for $B \gg B_{nuc}$ and $P_S(\tau_S) = 1 - \frac{3}{4}C_2\left\{1 - \frac{1}{9}\left(1 - 2e^{-\frac{1}{2}(\tau_S/T_2^*)^2}\left\{(\tau_S/T_2^*)^2 - 1\right\}\right)^2\right\}$ for $B \ll B_{nuc}$. A fit to the 100-mT data gives $C_1 = 0.62 \pm 0.01$ and $T_2^* = 10 \pm 1$ ns. A fit to the $B = 0$ data with $T_2^* = 10$ ns fixed gives $C_2 = 0.74 \pm 0.01$.
32. We have verified that the system is in the ground state of the nuclear fields by varying the pulse parameters τ_S and τ_S'. No dependence on these parameters was observed when varied as in the singlet-triplet spin-echo measurements.
33. Two synchronized Tektronix AWG710B pulse generators were used for the fast Rabi measurements.
34. C. P. Slichter, *Principles of Magnetic Resonance* (Springer-Verlag, Berlin, ed. 3, 1996).
35. L. M. K. Vandersypen, I. L. Chuang, *Rev. Mod. Phys.* **76**, 1037 (2004).
36. F. H. L. Koppens *et al.*, *Science* 27 July 2005 (10.1126/science.1113719).
37. W. A. Coish, D. Loss, available at www.arXiv.org/abs/cond-mat/0506090 (2005).
38. L. A. Wu, D. A. Lidar, *Phys. Rev. Lett.* **88**, 207902 (2002).

39. We acknowledge useful discussions with S. Das Sarma, H.-A. Engel, X. Hu, D. Loss, E. Rashba, and P. Zoller. Funding was provided through the Army Research Office under grants DAAD55-98-1-0270 and DAAD19-02-1-0070; the Defense Advanced Research Projects Agency–Quantum Information Science and Technology program; NSF under grant DMR-0072777; the NSF Career Program; the Harvard Center for Nanoscale Systems; and the Sloan and Packard Foundations.

5 July 2005; accepted 22 August 2005
Published online 1 September 2005;
10.1126/science.1116955
Include this information when citing this paper.

Coherent Manipulation of Coupled Electron Spins in Semiconductor Quantum Dots

J. R. Petta *et al.*

Science **309**, 2180 (2005);
DOI: 10.1126/science.1116955